Application for Sun Pharma Science Foundation – Science Scholar Award'2021

Title of the research work:

Development of a polysaccharide-based, *in-situ* forming, self-healing, ECM-mimetic scaffold to modulate cellular response for an enhanced wound healing

Name of the Applicant:

Swati Sharma
PhD Scholar,
Department of Pharmacy,
Birla Institute of Technology & Science, Pilani

Development of a polysaccharide-based, *in-situ* forming, self-healing, ECM-mimetic scaffold to modulate cellular response for an enhanced wound healing

Introduction

The incidence of chronic non healing wounds is on the rise worldwide, resulting in impaired mobility, systemic infections, or even death in the patients. 1% to 2% of the total population in developing countries is estimated to experience a chronic wound during their lifetime which sometimes leads to death [1]. The current state-of-the-art treatment for chronic and severe wounds relies on hydrogels, films, gauge, foams, membranes, etc [2]. They mainly act as hemostatic, some of them additionally have anti-microbial property. However, none of the traditional wound dressings can improve cell proliferation and tissue remodeling, which are essential for wound healing. Henceforth, there is a need for the development of a wound dressing which may act on the complete healing process.

Skin regeneration is a complex process that requires a coordinated integration of multiple components at the wound site, among which the extracellular matrix (ECM) plays one of the most critical roles. ECM helps different cells, including keratinocytes, fibroblasts, smooth muscle, and endothelial cells, to migrate and proliferate to re-epithelialize the denuded wound surface [3]. However, in severe and chronic wounds, this ECM structure gets damaged, resulting in impaired wound healing [4, 5]. Without proper ECM support, damaged skin cells cannot proliferate and undergo senescence, leading to reduced epithelialization [6, 7]. In the absence of ECM, even an increased level of growth factors fails to improve wound healing, as observed in the non-healing chronic leg ulcers [8, 9], suggesting that the ECM structure plays a critical role in the wound healing process.

Understanding the ECM's importance in wound healing, multiple ECM mimetic scaffolds have been developed previously [10, 11]. However, almost all of the clinically available scaffolds are prefabricated by design [12, 13]. Preformed scaffolds have several logistic issues associated with their use, including complicated fabrication, handling, and packaging. Furthermore, the most important limitation of a preformed scaffold is its inability to interact with the denuded wound bed's basal skin cells. Prefabricated scaffolds do not penetrate to the uneven wound bed due to their stiffness, making their interaction with the basal skin cells to a minimum [14]. It would be highly beneficial if a scaffold can be developed, which will be liquid during application, helping it percolate to the wound's deepest crevices; however, after application, it becomes a porous mesh-like structure optimally supporting cell growth and function.

A unique way of developing an in-situ scaffold is by crosslinking a polymer at the wound site. The problem with the chemical crosslinking process is that it produces chemical byproducts, which are toxic for an open wound. Also, the development process is complex, making the scale-up process complicated and clinical utilization difficult. An ingenious way of making an in-situ crosslinked polymer is by using the poly-electrolyte complexation (PEC) strategy. In this

approach, two oppositely charged poly-electrolyte polymers interact to form a scaffold almost instantaneously, without using chemical crosslinking agents, thereby making the process very simple and straightforward and free from any toxic chemicals. We have developed such an *in-situ* forming scaffold by simple mixing of high molecular weight chitosan (CH; positively charged polysaccharide) with low molecular weight chondroitin sulfate (CS; negatively charged polysaccharide). The uniqueness of this scaffold is, it can be applied as a solution at the wound bed, and after application, would spontaneously crosslink to form a porous scaffold at the wound site *in-situ*, thereby reaching to the deepest part of the wound and providing support to the wound bed cells (**Fig 1**).

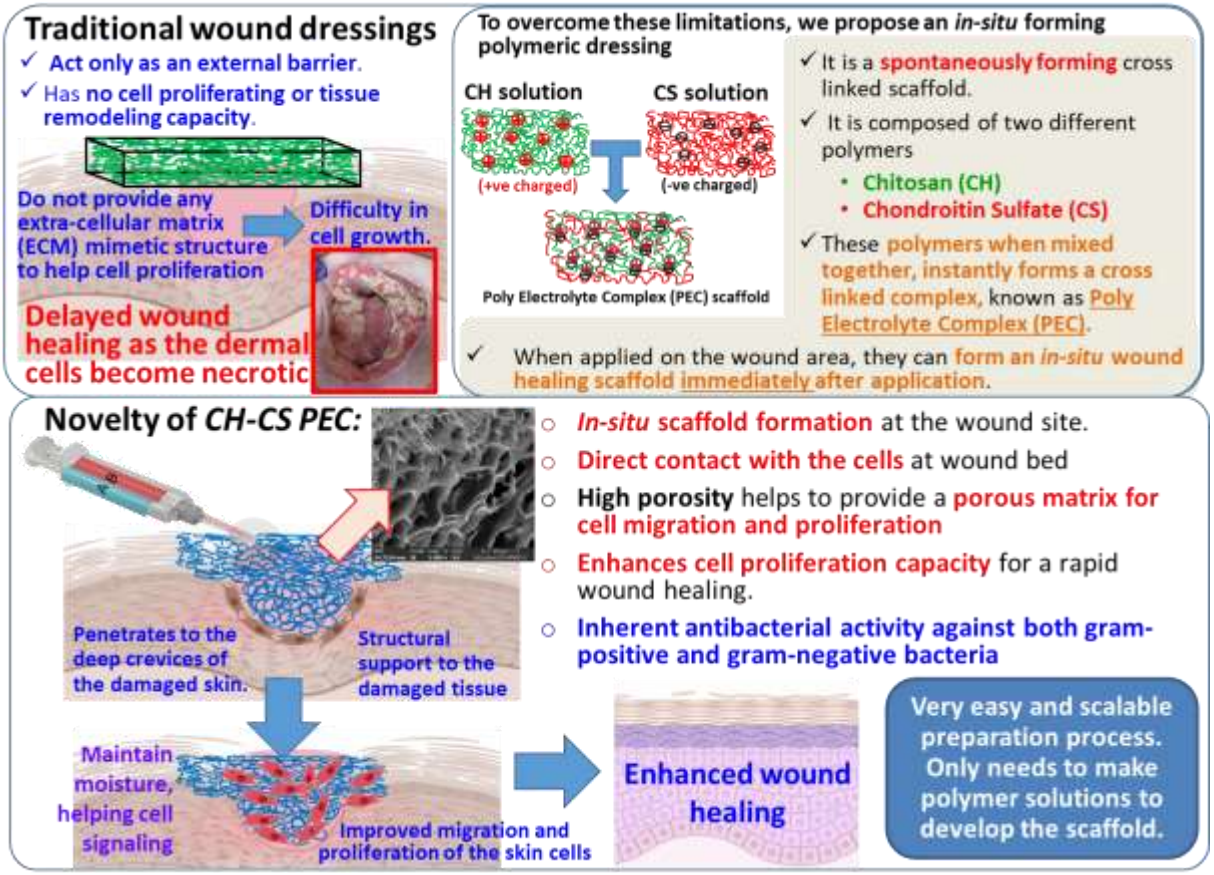

Figure 1: The significance of the proposed technique.

We have further loaded simvastatin, a proangiogenic drug to the scaffold for the possible clinical use. Simvastatin is a widely used lipid lowering agent but at low concentration it aids to secrete vascular endothelial growth factor and promotes angiogenesis. The aim of this study is to develop a drug-loaded, *in-situ* forming scaffold, which could act on all the cell types involved for wound healing, and with easy scalability and translational value.

OBJECTIVE OF THE PROPOSED RESEARCH

1. Fabrication of Chitosan- Chondroitin sulfate polyelectrolyte complex scaffold and loading a suitable drug (Simvastatin) in an optimized CH-CS PEC.
2. Determination of the cellular efficacy for the wound healing activity of the CH-CS PEC on different cell types involved in the healing process, *in-vitro*. Determination of functional efficacy of simvastatin loaded polymeric micelles.
3. *In-vivo* wound healing study and determination of the *in-vivo* mechanism involved in the wound treated with both CH-CS PEC and simvastatin-loaded CH-CS PEC.

METHODOLOGY

Objective 1: Fabrication of Chitosan- Chondroitin sulfate polyelectrolyte complex scaffold and loading a suitable drug (Simvastatin) in an optimized CH-CS PEC.

1. Optimization of CH-CS PEC:

CH-CS PEC was prepared using electrostatic crosslinking method. Solutions of polymers were separately prepared by solubilizing CH in 1% w/v glacial acetic acid solution and CS in distilled water. CH solution was then dialyzed using a 10 kDa cut-off membrane against MQ water to remove the acetic acid and sterilized by autoclaving, whereas CS solution was sterilized by filtration. CH of different molecular weight and volume ratios of CH and CS were prepared to optimize the CH-CS PEC. The CH-CS PEC was lyophilized for further characterization.

- **Incorporation of Simvastatin polymeric micelles to the CH-CS PEC.**

For effective loading and controlled release of simvastatin from CH-CS PEC we prepared Simvastatin polymeric micelles. These were prepared by rotory flask evaporation method. Briefly, Soluplus and vitamin E-TPGS ratio (4:1) and simvastatin were solubilized in acetone together and were vacuum dried using rotory flask eveaporator to make a thin film. The polymeric film was then rehydrated in water. The obtained polymeric micelles were then centrifuged at 25000RPM for 20 mins to remove free drug. The micelles were then loaded int the CH-CS PEC by using double barrel syringe.

2. Characterization of CH-CS PEC complex:

- **Physicochemical characterization of CH-CS PEC:**

CH-CS PEC was fabricated by mixing CH and CS solution together undergoing electrostatic interaction. It was characterized by analyzing the FTIR, solid state NMR, X-ray diffraction and thermal degradation studies of CH-CS PEC and its comparison with pure CH and CS. The complexation was confirmed by change in the peak of the CH-CS PEC in compare to pure CH and CS.

- **Swelling and Porosity Studies:**

Pre-weighed CH-CS PEC scaffold was immersed in PBS (pH 7.4). The weight of the prepared PEC was calculated at different time points till 5 h. Swelling ratio was calculated by:

Swelling ratio= $((W_w - W_i)/W_i) \times 100$

Where W_i was the initial weight of the sample and W_w was the wet weight of the samples at the respective time interval. Porosity of the CH-CS PEC was performed by alcohol displacement method as wellas was confirmed by scanning electron microscopy.

- **Rheological characterization of CH-CS PEC:**

Rheological measurements were performed on Anton Paar's (MCR 92) rotational rheometer, using a plane plate (PP25), 25 mm in diameter. The samples were loaded on the disc, putting a gap of 1 mm between the disc and PP25. Oscillatory amplitude and frequency sweep tests were performed to study the viscoelastic nature of the scaffold. The amplitude sweep test was performed at a constant frequency of 100 rads/s to find the scaffold's linear viscoelastic region (LVER). After confirming the LVER region, the frequency sweep test was performed within the LVER limit. The viscoelastic behavior was analyzed in terms of storage modulus (G') and loss modulus (G"). Further, the thixotropic analysis of the scaffold was performed by evaluating the recovery rate at different strains. In that study, change in viscosity was evaluated at initial strain of 0.25% for 10s, 1000% strain for 10s, and then 0.25% strain for a further 200s. Also, a macroscopic evaluation of the self-healing property of CH-CS PEC was performed. The CH-CS PEC was prepared as two separate disc-shaped scaffolds, amongst which one was stained with Rhodamine B. Both the discs were kept in surface contact for 3 min; after that, their physical integrity was evaluated and photographed.

- **Biochemical estimation of CH-CS PEC:**

As the wound is expected to act as a hemostatic agent, checking its blood compatibility is one of the important criteria. To check the blood compatibility of the CH-CS PEC with blood the in-vitro hemolysis assay was performed as per the method described in the article by hu et al. [15]. The hemolysis study was performed in the RBCs isolated from the rat blood. Further the blood clotting study was performed as per the protocol mention in the article by Yeu et al. The study was performed to check the hemostatic potential of the proposed wound dressing.[16]. Further to check the thrombotic property of the proposed wound dressing, Protein adsorption was performed using bovine serum albumin as the standard protein by batch contact method. [17]

Antibacterial activity of CH-CS PEC:

Chitosan as an antimicrobial agent is well documented.[18] Hence we want to check the antibacterial activity of the prepared CH-CS PEC. The study was performed using micro-broth dilution method using tetraphenyl tetrazolium chloride (TTC) dye. The experiment was performed on *Pseudomonas aeruginosa* strains. [19]

3. Characterization Simvastatin micelles:

Micelle size (hydrodynamic diameter) and PDI were analyzed by dynamic light scattering (DLS), using Malvern Nano ZS (Malvern's instrument Ltd., UK) at 25 °C. A dilute suspension of micelles was used to determine the size (dilution was optimized to obtain consistent and reliable readings). Morphology of the micelle was analyzed by Scanning Electron Microscopy (SEM). Micelle suspension was placed on a glass coverslip and air-dried. The glass coverslips were dropped onto a double-sided carbon tape attached to the sample stub and coated under vacuum with gold in an argon atmosphere for about 45 s. Then morphology was examined by scanning at 20kv with SEM.

To calculate the percent encapsulation efficiency (%EE) and percentage drug loading (%DL), 1 ml of the micelles were centriguged at 17000RPM for 20min. The supernatant was removed and the remaining micellar pellet was solubilized in 1 ml acetonitrile and vortexed for 5–10 min. Then the resulted solution was injected into HPLC, and the concentration of simvastatin was analyzed using a calibration curve prepared by using the developed simvastatin analytical method

%EE = weight of the drug in the micelles / initial weight of drug × 100

%DL was calculated by the formula:

%DL = weight of the drug in the micelles / total weight of the micelle

For the in-vitro release study, the prepared simvastatin micelles were loaded into the CH CS PEC. Micelles equivalent to 500ug/ml was loaded to the CH-CS PEC and the drug release was performed in the franz diffusion cell apparatus. The release media used was 10mM phosphate buffer solution (PBS) with 1% tween 80 was used to maintain the sink condition. The % drug release was carried out till 24h.

Objective 2: Analysis of in-vitro efficacy of CH-CS PEC on keratinocyte, fibroblasts and macrophages. Determination of pro-angiogenic potential of simvastatin loaded CH-CS PEC on Endothelial cells.

1. Cell Proliferation and migration:

To study the functional efficacy of fibroblasts and keratinocytes initially the cell proliferation study was performed by seeding the Keratinocyte cells (HaCaT cell line) and Human dermal fibroblasts (HDF) cells on the CH-CS PEC. The cell density was observed under fluorescent microscope after staining the cells at specific time points with DAPI stain. Proliferation was further confirmed by real time qPCR analysis. . For the cell migration assay, the cells were seeded on the scaffold coated (CH-CS PEC, CH, and CS) culture vessel supported with μ-dish culture insert (ibidi insert, Martinsried, Germany). Cells grown on plain culture vessel (TPP-Techno Plastic Products AG., Trasadingen, Switzerland) were used as control. When the cells become confluent, culture inserts were slowly removed without disturbing the edge to mimic the wound. Cells were photographed at various time laps periods (0, 8, 16, and 24 h). All the samples were observed at 20× magnification. The rate of cell migration (mm) in various groups was calculated by using Image J software (NIH, Washington, USA). Live cell migration was recorded by time-lapse video device (Cyto smart-II, Lonza, Inc., Morristown, NJ, USA).

2. In-vitro cellular expression of wound healing markers treated with CH-CS PEC:

According to the stages involved in the healing process we planned to study the expression of various functional markers for HaCaT and HDFs were performed using qPCR in the cells treated with the drug loaded CH-CS PEC. The primers was designed using primer blast. Total RNA was isolated using TRIzol™ Reagent (Invitrogen™). 5µg of total RNA from each sample was subjected to cDNA synthesis using SuperScript® III Reverse Transcriptase kit (Life technologies). Each cDNA sample was amplified using Power SYBR Green (Applied Biosystems™ PowerUp™ SYBR™ Green Master Mix). Each cycle will consist of denaturation of 95°C for 15 seconds, annealing at 60°C for 15 seconds and extension at 72°C for 1 min. Each cycle was followed by dissociation curves for every sample. GAPDH was used as an endogenous control to normalize each sample.

Further, expression of proliferating cell nuclear antigen (PCNA), as cell proliferation marker was analysed by western blotting. Cells was treated with drug loaded CH-CS PEC for 48h. Thereafter, cells was lysed in a modified RIPA buffer (Sigma-Aldrich; Merck KGaA), and the protein content was measured using the Bradford reagent. Then, the loading buffer was added to the lysates followed by heat denaturation (100˚C for 10 min) and cooling on ice. Equal concentrations of protein lysates was loaded in denaturingpolyacrylamide gels and thereafter was transferred to polyvinylidene fluoride (PVDF) membranes (Thermo Fisher Scientific, Inc.; cat. no. 88518) for blocking with 5% skimmed milk (HiMedia; Mumbai, India; cat. no. GRM1254). The blots was probed with specific primary antibody at dilution of 1:1,000, GAPDH was used as a loading control. The secondary antibody was used at dilution of 1:10,000. The protein intensity was detected using an enhanced chemiluminescence detection system (Thermo Fisher Scientific, Inc.). The expression levels was densitometrically quantified using ImageJ software (National Institutes of Health, Bethesda, MD, USA) and normalized to the control

3. Development of in-vitro infection model:

Chitosan is reported to be antibacterial due to its cationic charge. Hemce we wanted to study the effect of CH-CS PEC on macrophages when infected with the *Pseudomonas aeruginosa* bacteria. RAW 264.7, a murine macrophage cell line was used for the study. Briefly, Raw 264.7 were grown on the CH and CH-CS PEC in a density of 1x 10^5 cells. Post 24 hour of incubation, The cells were infected with bacteria for 3h and 6h. The phagocytic ability, Cytokine secretion and the functionality of infected bacteria was further studied by microscopy studies and qPCR.

4. Determination of pro-angiogenic potential of simvastatin loaded CH-CS PEC:

For the determination of angiogenesis, EAHy926, human endothelial cell line will be used. The simvastatin dose confirmation was done by performing the cytotoxicity assay. For the determination of angiogenesis, Tube formation assay will be performed on the endothelial cells followed by evaluating the expression of VEGF by qPCR analysis.

Objective 3: In-vivo wound healing study and determination of the molecular mechanism involved in the wound treated with simvastain loaded CH-CS PEC.

1. Development of the rat incisional wound model.

All animal experiments were conducted following the regulation of the Animal Ethics Committee, BITS-Pilani (Protocol number: IAEC/RES/25/3). The *in-vivo* wound healing study was performed in the Wistar rats with a full-thickness excisional wound of 2×2 cm^2 area. Four groups were included in the study: i) control (untreated), ii) lyophilized CH-CS PEC (as a preformed scaffold), iii) *in-situ* CH-CS PEC, and iv) a market available CH based preformed scaffold. *In-situ* CH-CS PEC treatment was given through a custom-made double-barreled syringe, with CH solution in one chamber and CS solution in the other chamber. For application, both the pistons of the double-barreled syringe were compressed simultaneously, leading to the ejection of both the solutions at the same rate using a custom-made double-barreled syringe. The solutions were mixed in the wound bed itself, leading to the formation of the *in-situ* scaffold. The wound healing was analyzed by taking the images of treated wounds every second day. Further histology and Immunohisctochemistry was performed by collecting the skin after the treatment completion.

Development of Chronic wound model:

After establishing the efficacy of CH-CS PEC we wanted to develop The Chronic wound model for the determination of functional efficacy of simvastatin loaded CH-CS PEC. Initiallly, The animals will be given a single dose of streptozotocin (50 mg/kg), i.p. to induce Type-I diabtetes. After four days post injection, glucose levels of the animals will be evaluated using the Accucheck Active, Glucometer. The animals with glucose level > 250mg/dl will be considered diabetic and further incision wound will be created on the animals in the similar way as discussed previously. The Histology and immunohistochemistry of the skin samples will be performed after the end of the study.

Statistical analysis

The data were analyzed using GraphPad Prism software version 8. Comparison among data sets was statistically determined using one-way or two-way ANOVA; posthoc Tukey's test was performed to compare each group's means with every other group. Data were represented as mean ± SD.

Results:

Objective 1: Fabrication of Chitosan- Chondroitin sulfate polyelectrolyte complex scaffold and loading a suitable drug (Simvastatin) in an optimized CH-CS PEC.

1. Physicochemical Characterization of CH-CS PEC.

To confirm the formation of CH-CS PEC, FTIR, XRD, thermal degradation and solid state NMR were performed. As the PEC was insoluble in any solvent, solid-state 13C NMR was performed to confirm the CH-CS PEC formation. CH is composed of β-(1,4)-[2-amino-2-deoxy-β-D-glucan], whereas CS is an alternating copolymer of D-glucuronic acid and N-acetyl-D-galactosamine, joined through β-(1,3) linkages. As depicted in **Fig. 2A,** the CP MAS 13C spectra of CH showed characteristics peaks at 105.899 ppm corresponds to the carbon atom at C1 position, 85.494 ppm

for carbon atom at C4, 76.236 ppm for C5 and C3 carbon atoms, and at 61.678 and 58.024 ppm, two convoluted peaks are observed, which were attributed to carbon C6 and C2 [20]. Similarly, the CP MAS 13C spectra of CS exhibited peaks at 103.340 ppm corresponding to C1 carbon atom, convoluted peaks between 77.169 ppm and 74.165 ppm corresponds to C3 and C4 carbon atoms, 69.170 ppm for the C5 carbon atom of the glucuronic acid moiety. C2 carbon atom showed a peak at 52.055 ppm, and 24.463 ppm depicts the N-acetyl methyl group's peak. [21]. CH and CS were hypothesized to crosslink by electrostatic interactions between the $–NH_2$ group of CH and the –COOH group of CS to form the CH-CS PEC. The peak corresponding to C2 carbon atom of CH at 58.024 ppm exhibited a shift in the CH-CS PEC to 57.476, which may be due to the interaction of the $–NH_2$ group attached with the C2 carbon. Similarly, the peak assigned to the C5 carbon atom of the glucuronic acid moiety of CS at 69.170 ppm disappeared in the CH-CS PEC (**Fig. 2A**). This data confirmed the interaction of the –COOH group of CS with the $–NH_2$ group of CH in the CH-CS PEC. Further, The X-ray diffraction pattern of CH, CS, and CH-CS PEC was performed to evaluate the change in crystallinity after complexation (**Fig. 2B**). The CH showed a characteristic sharp peak at 19.99° [22], indicating the crystallinity of CH, while CS showed a broad peak at 20.19° [23]. All these peaks were found to disappear in the CH-CS PEC, indicating formation of an amorphous, crosslinked structure. During the PEC formation, CH and CS complex with each other through electrostatic interaction, leading to a loss of the ordered, crystalline structure in the crosslinked scaffold. Similar observation has been made with other PECs as well [24]. Thermal gravimeteric analysis and Differential scanning calorimetry were performed to study the thermal behaviour of the CH-CS PEC and individual polymer. The data corroborated with the resuts of solid state NMR and XRD. To further confirm the complex formation FTIR was performed to study the change in the intensity of the functional group peak. The FTIR results also showed formation of anide bond with reduced intensity of sulfate peak in CH-CS PEC indicating complex formation.

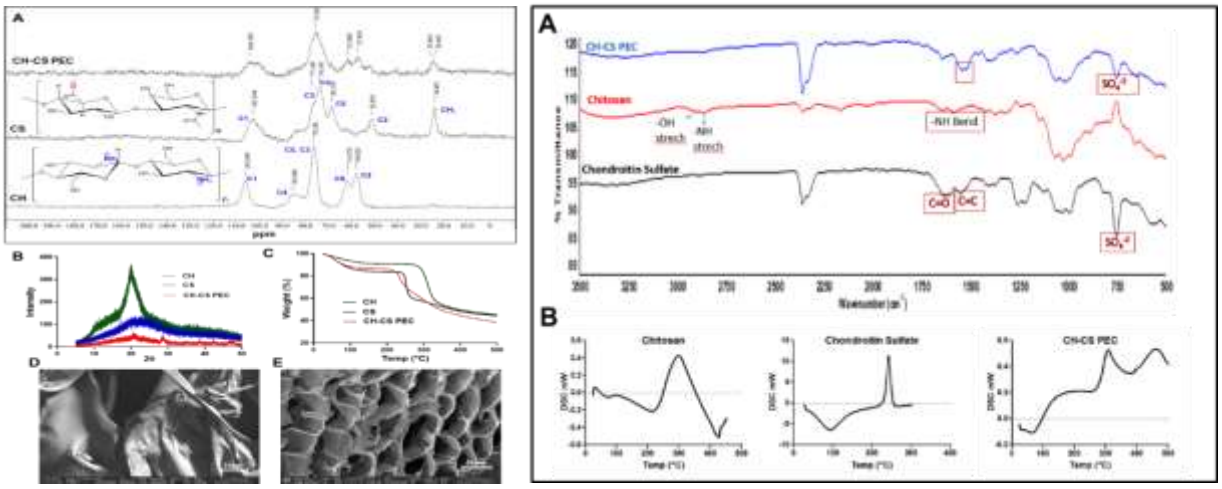

Fig. 2. Physicochemical characterization of the CH-CS PEC. **A**: Solid-state CP MAS 13C NMR of CH, CS, and CH-CS PEC. **B**: XRD analysis of CH, CS, and CH-CS PEC. **C**: TGA analysis of CH, CS, and CH-CS PEC. **D**: FE-SEM image of CH. **E**: FE-SEM image of CH-CS PEC **F.** FTIR analysis of CH,CS and CH-CS PEC, **G**. DSC analysis of CH, CS and CH-CS PEC.

Optimization of the CH-CS-PEC by evaluating % swelling and Porosity:

After confirming that CH and CS can spontaneously interact to produce a PEC, we wanted to determine the best ratio of CH and CS to produce the most useful scaffold to be used for wound healing purpose. To find out the best ratio of CH and CS, Box Behnken design was chosen for the optimization of CH-CS-PEC. Based on our preliminary experiment and understanding, three independent variables were chosen for optimization, concentration of CH, concentration of CS and MW of CH. Three different concentrations and MW was selected, as depicted in **Table 1**. These variables were used with Design Expert software (version 8.0.0.7) to construct the design matrix (**Table 1**). Based on this design matrix, PEC was prepared and tested for their efficacy. We have chosen swelling and porosity as the quality target product profile (QTPP) as these two properties are essential requirements of a wound dressing material. Higher swelling and property defines that the dressing will absorb wound exudates, promoting wound healing. The swelling and porosity of different batches of PEC is depicted in **Table 1.** Among the three variables, MW of CH was found to have the most significant impact on the QTPP of the CH-CS-PEC and high MW showed enhanced swelling and porosity compared to the low and medium MW CH. This may be due to the longer chain length of the high MW CH, which increases the entanglement of the polymer, increasing porosity. The effect of MW of polymer on the porosity of PEC has been studied before and similar phenomenon has been observed.[25] Other two variables, namely concentration of CH and concentration of CS, were found to have moderate effect on the QTPP, and higher concentration of both CH and CS generally increased the QTPP slightly. We also found that more than 5 wt % of high MW CH was very difficult to dissolve, and with increase in the concentration of CS beyond 5 wt %, though there was a slight increase in swelling, there was decrease in porosity. Based on the observed effect of the influence of MW of CH, and concentration of both CH and CS on the properties of the CH-CS-PEC, we have selected high MW CH and 5 wt% concentration for both CH and CS for our further study.

Table 1: Quality target product profile of chitosan-chondroitin sulfate PEC

Batches	Factor			Responses	
	X_1 Concentration of Chitosan	**X_2 Concentration of chondroitin sulfate**	**X_3 MW of CH**	**Swelling Study (%)**	**Porosity (%)**
1	5	2	Low	219.055	22.45247
2	5	8	High	928.977	104.2015
3	8	5	High	**Batch not formed**	
4	5	5	Medium	345.045	56.78634
5	8	2	Medium	385.233	65.05915
6	8	8	Medium	232.23	70.17529
7	2	5	High	879.4945	81.49207
8	5	2	High	865.12	108.6517
9	2	2	Medium	247.625	76.77016

10	5	8	Low	234.67	28.84345
11	8	5	Low	235.71	20.41825
12	2	5	Low	167.76	18.08617
13	2	8	Medium	278	20.76

2. Rheological characterization of CH-CS PEC:

To be useful as a wound dressing material, the electrostatically crosslinked CH-CS PEC should have sufficient viscoelastic properties. The matrix's viscoelasticity determines the primary cellular responses like cell adhesion, cell spreading, and cell proliferation [26]. The viscoelasticity of the CH-CS PEC scaffold was evaluated with respect to the storage modulus (G`) and loss modulus (G``). The storage modulus (G`) describes the elastic response of the solid material and depicts the degree of crosslinking in the scaffold, while the loss modulus (G``) determines the viscous, irreversible response resulting in the deformation [27]. Oscillatory tests, namely amplitude and frequency sweep tests, were performed to analyze CH-CS PEC's viscoelastic behavior. The initial step to study viscoelasticity is to determine the linear viscoelastic region (LVER). CH exhibited a significantly lower value of G' (~60 Pa, **Fig. 3A**), than that of G`` (~90 Pa), indicating the fluidic nature of CH. Low G` of CH has been reported earlier as well [28]. On the other hand, CH-CS PEC exhibited a significantly higher G` (~17000 Pa) compared to G`` (~7800 Pa), which indicated better crosslinking and mechanical strength (**Fig. 3B**). The LVER for CH-CS PEC was found to be 3.5% shear strain. We have also studied the changes in viscoelasticity of CH-CS PEC with a frequency sweep test. As CH exhibited lower G` than G`` in the amplitude sweep test, indicative of no crosslinking, it was excluded from the frequency sweep test. The study was performed below the LVER region, at a constant shear strain of 1%, with a change in frequency from 0.1-100 rad/s. Here also, a significantly higher G` value was detected compared to the G`` with the CH-CS PEC, indicating considerable structural rigidity of the scaffold (**Fig. 3C**). The G` value was gradually increasing from ~9800 Pa to ~21600 Pa with the increase in angular frequency. The increase in the G` indicated that the electrostatic crosslinking within the polymer matrix acted like fixed network junctions, increasing the ability of the crosslinked scaffold to store the applied energy, leading to elastic-like characteristics. High elasticity of a matrix has been reported to support cell proliferation and migration [29]. A significant increase in the G` with the CH-CS PEC compared to CH alone implied that when CH is mixed with CS, a strong ionic crosslinked scaffold was formed with good stability and viscoelasticity.

Next, we studied the CH-CS PEC's self-healing property by performing the thixotropic study at different level of strains. The study was performed at 0.25% strain for 10s and 1000% strain for 10s and then the recovery was observed at 0.25% strain for 200s by measuring the change in viscosity. The results depicted low initial viscosity with CH (1643 mPa.s at 0s at 0.25% strain) compared to CH-CS PEC (404000 mPa.s at 0s at 0.25% strain) (**Fig. 3D and E**). Higher viscosity with the CH-CS PEC indicated a crosslinked structure. While applying 1000% strain for 10s, a highly significant decrease in the viscosity was observed with both CH and CH-CS PEC. In the

recovery stage at 0.25% strain, CH exhibited a moderate increase in the viscosity (40% of the initial), however, a rapid and significant increase in the viscosity was observed with the CH-CS PEC with more than 90% recovery to the earlier level. Rapid recovery in the viscosity indicated quick restoration of the crosslinked structure in the CH-CS PEC. The self-healing ability was further confirmed by macroscopic evaluation. In this study, the CH-CS PEC was prepared in two discs. One of the discs was stained with Rhodamine B dye, the other kept as colourless. Then both the CH-CS PEC disc were kept in close contact. After 3 min, both the disks formed deep interconnection within themselves, depicting the CH-CS PEC's efficient self-healing and adhesive potential (**Fig. 3F**). As the scaffold was formed due to ionic interactions, if disrupted, they can quickly regenerate due to rapid ionic bond formation, unlike covalent bonds. This self-healing property has been observed with other polyelectrolyte complexes as well [24]. Disruption of the scaffold structure's integrity due to body movements can reduce the efficacy of the scaffold. The development of a self-healing scaffold that can automatically repair the damage without external intervention can be highly beneficial [30, 31].

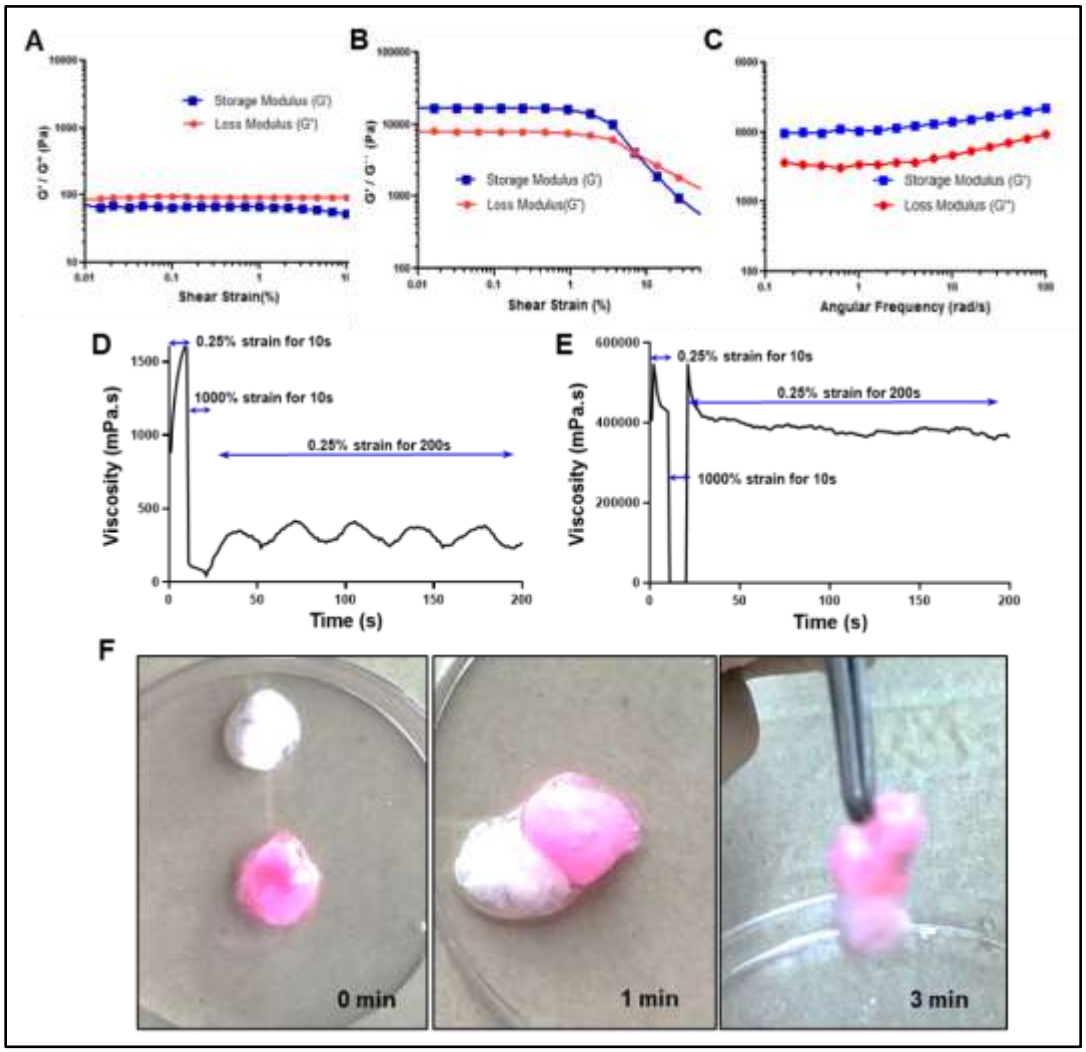

Fig. 3. Rheological characterization of the CH gel and CH-CS PEC. **A**: Amplitude sweep test for CH and and **B**: CH-CS PEC. The graph depicts the change in storage modulus (G') and loss modulus (G'') with a change in the shear strain at an angular frequency of 100rad/s. **C**: Frequency sweep test for CH-CS PEC depicting the change in G' and G'' with a change in angular frequency from 0.1- 100 rad/s within the LVER region. **D**: Thixotropic analysis of CH and **E**: CH-CS PEC. The graph depicts the change in the viscosity at different % strain. **F**: Macroscopic evaluation of the self-healing property of CH-CS PEC.

3. Biochemical estimation of CH-CS PEC:

Biocompatibility is one of the most important properties of a wound-healing scaffold. As they directly come in contact with the blood, hematological stability is a good indicator of their biocompatibility. It is regarded that lower hemolysis is an indicator of better blood compatibility [32]. According to the American Society for Testing and Materials (ASTM), any material would be called non-hemolytic if it causes below 2% hemolysis.[33] We tested different concentrations of prepared CH-CS-PEC ranging from 2mg/mL to 0.008mg/mL.(**Fig.4(A)**) Maximum hemolysis was observed with 2mg/mL CH-CS-PEC at 1.26±0.45%. So the prepared CH-CS-PEC scaffold was considered as a non-haemolytic material. We further evaluated whole blood clotting and protein adsorption study to check the hemostatic potential of the CH-CS PEC. It is particularly important for the treatment of open wounds which are bleeding. Induction of thrombosis can arrest the bleeding and stop blood loss. We evaluated the hemostatic potential of the CH-CS-PEC and compared it with CH scaffold on the basis of its blood clotting index (BCI). Smaller value of BCI indicates stronger the hemostatic potential of the material. CH-CS-PEC demonstrated significantly higher hemostatic ability (**35.46% BCI**) compared to CH scaffold (**83.64% BCI**).**(Fig. 4(C)** The higher hemostatic ability of the CH-CS-PEC compared to CH scaffold may be due to the higher porosity and swelling of the CH-CS-PEC compared to CH. Blood cell adhesion study was performed using scanning electron microscopy. The samples were treated in the same manner as that of treated for the blood clotting studies. PEC treated with blood was fixed with 4% formaldehyde solution for 15 minutes and dried at 37°C. The SEM images of the blood pretreated scaffold of chitosan and chitosan-chondroitin sulfate showed that CH-CS PEC showed a better blood cell adhesion in compare to the scaffold prepared with chitosan alone. (Fig. 4 E and F)After demonstrating high hemostatic activity with the CH-CS-PEC, we wanted to find the underlying cause for this. It is generally accepted that the first step of thrombosis formation is the protein adsorption on the surface of the scaffold In agreement with the % swelling data, higher amount of BSA was found to be adsorbed on the CH-CS PEC than that of CH scaffold as the water uptake capacity of the CH-CS PEC is higher than that of CH alone.

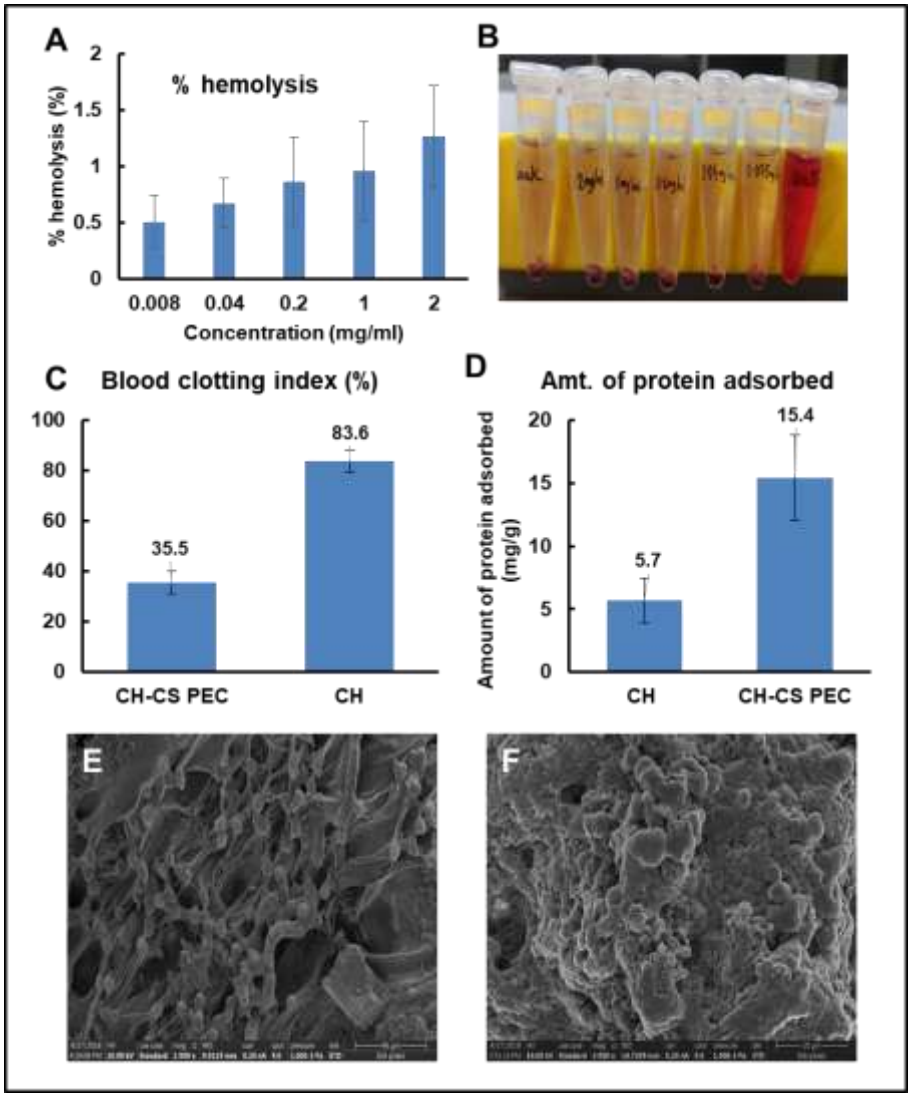

Fig. 4. Determination of hemocompatibility and hemostatic ability of CH-CS PEC. A. Hemolysis study. B. Pictorial representation of the hemolysis. C. Comparison of blood clotting index and D. protein adsorption on CH-CS PEC with that of CH scaffold. E. SEM image of blood cell adhesion on CH-CS PEC and F. that on the CH scaffold.

4. Antibacterial activity of CH-CS PEC:

Chitosan is reported to have antimicrobial activity due to its cationic nature. We tested the antibacterial activity of the CH-CS PEC in pseudomonas aeruginosa as the bacteria is involved in surface infections at the time of injury. The bacterial cell viability was confirmed on the basis of the intensity of formation of orange-red formazon crystals when the cells were treated with TTC dye. The bacteria treated with CH-CS PEC showed high bacteria cell death after 24h of incubation. In compare to CH and CS (**Fig 5B**). We further evaluated the zeta potential of the untreated bacteria and bacteria treated with CH, CS and CH-CS PEC to check the membrane integrity. The results demonstrated changes in the membrane integrity as there was increase in the zeta potential with CH- CS PEC (-3.65mV). [34]

The SEM image of the bacteria treated with CH-CS PEC corroborates with the zeta potential data.

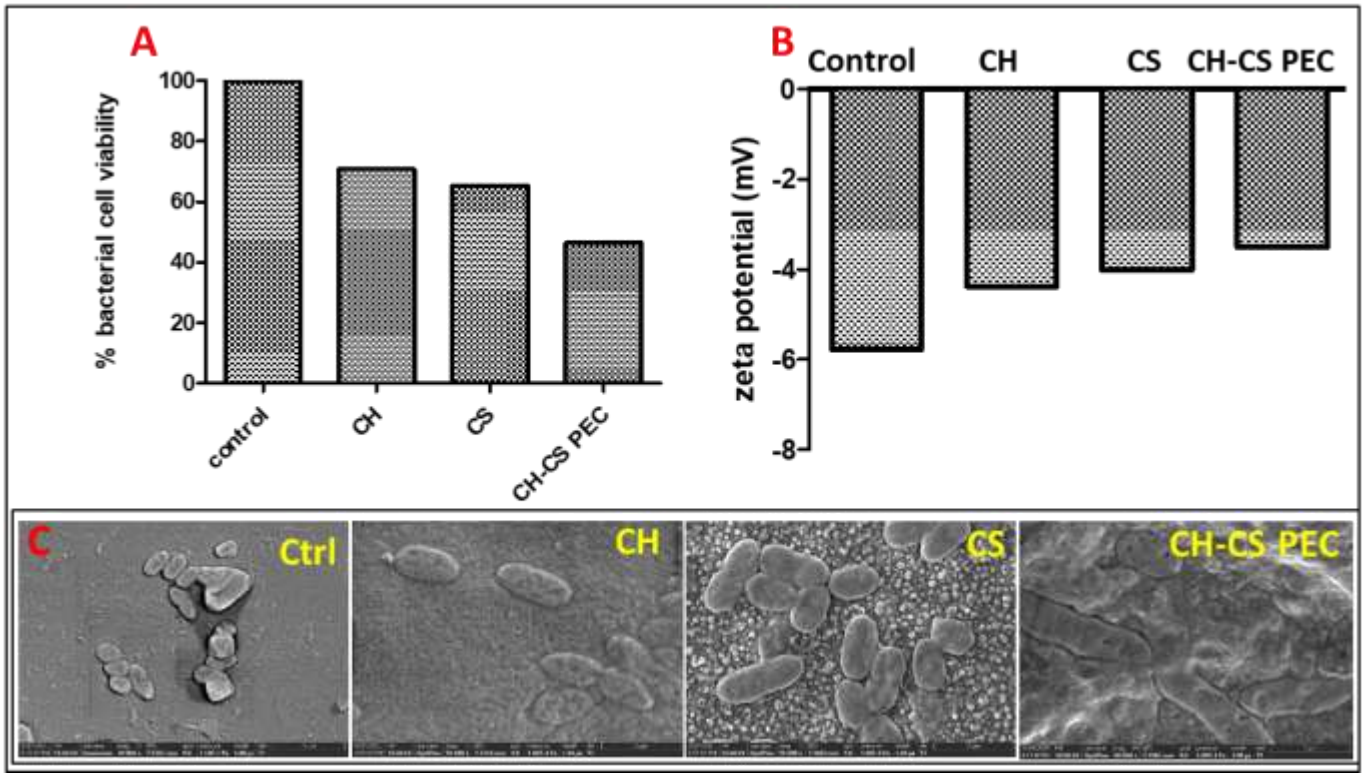

Fig 5: **A)** % bacterial cell viability of the bacteria when treated with CH, CS and CH-CS PEC, **B)** Membrane potential of the bacteria untreated and treated with CH, CS and CH-CS PEC. **C)** SEM imaging of bacteria treated with CH, CS and CH-CS PEC.

5. Incorporation of Simvastatin micelles to the CH-CS PEC

Simvastatin mixed micelles were prepared by taking soluplus and Vitamin E TPGS in the ratio of 4:1. The particle size of the drug loaded micelles was found to be 89.54nm±10.69. The particle size obtained by the DLS technique corroborates with the SEM imaging of the micelles. Different techniques were used to load simvastatin micelles into CH-CS PEC amongst which Miclees mixed in the CH gel and then fabrication of CH-CS PEC gave less drug loss and effective loading. (5.25 ±3.64% drug loss). (**Fig 6 C)** The entrapment efficiency of the simvastatin in the micelles was 89.21%±1.52 with 8.56% DL. Followed by effective loading of the miceels in the CH-CS PEC we checked the Drug release of drug loaded CH-CS PEC and compared it with only simvastatin micelles and pure API. We found controlled release in the drug loaded CH-CS in compare to normal micelles and pure drug.(**Fig 6D).** The further angiogenic potential of the Simvastain loaded CH-CS PEC on EAHY926 cell line and in-vivo efficacy on cheonic wound model is under progress

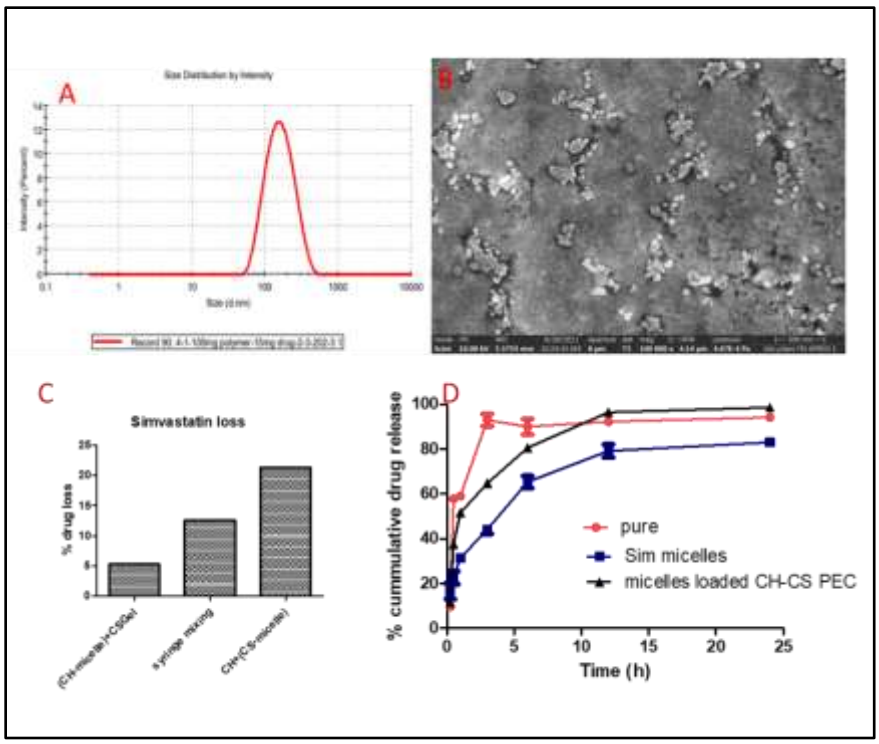

Fig. 6 A) Particle size distribution oif Simvastatin polymeric micelles, B)Scanning electron microscopy of the Simvastatin micelles, C) Micelle loading to the CH- CS PEC with different techniques and D) In-vitro drug release profile of simvastatin micelles loaded CH-CS PEC.

Objective 2: Analysis of in-vitro efficacy of CH-CS PEC on keratinocyte, fibroblasts and macrophages. Determination of pro-angiogenic potential of simvastatin loaded CH-CS PEC on Endothelial cells.

1. Cell Proliferation and Cell migration studies:

Enhanced proliferation and migration of the dermal and epidermal cells is one of the primary criteria for successful wound healing. It has previously been demonstrated that viscoelastic scaffolds can provide mechanical support to the cells, augmenting its proliferation rate [26, 35]. To evaluate the effect of the CH-CS PEC scaffold on the proliferation, we first evaluated the migration potential of both HaCaT and HDF cells, by wound healing assay. In the wound healing assay, significantly improved migration was observed in both HaCaT and HDF cells when grown on the CH-CS PEC, as depicted in **Fig. 7A** and **B** Cells grown on CH and CS exhibited similar migration to that of control cells grown on a petri dish. The rate of migration was found to be better in HDF than in the HaCaT cells.

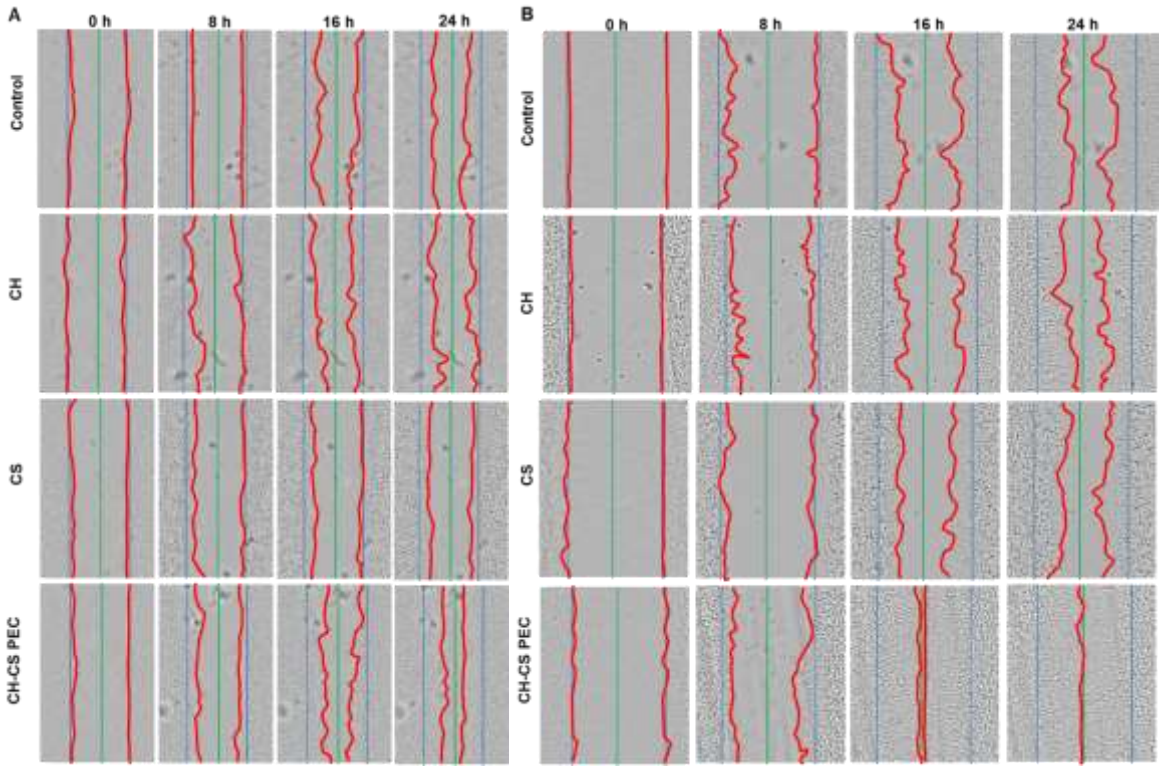

Fig. 7. *In-vitro* wound healing assay with HaCaT (**A**) and HDF (**B**) cells. Time-lapse microscopic images of the cells after incubating them for specific time points (0, 8, 16, and 24 h) with different polymeric scaffolds. Cells grown on the petri plate were used as the control. **Blue line:** starting point of cell migration. **Green line:** middle point of cell migration. **Red line:** migratory cell edge. Photographs were taken in bright field microscope with magnification of 20×. The quantitative analysis of the migratory potential of these cells is depicted in **Fig. 7A and B**. In both the cell types, a significant increase in migration was observed with the CH-CS PEC than other treatments. The average distance migrated by the HaCaT cells was found to be 0.53 ± 0.05 mm when grown on the CH-CS PEC, compared to 0.40 ± 0.04 mm with CH, 0.34 ± 0.02 mm with CS, and 0.40 ± 0.03 mm in the control cells after 24 h (**Fig. 8A**). Similarly, in the case of HDF, after 24 h, the average migration was 1.12 ± 0.06 mm with the CH-CS PEC, compared to 0.73 ± 0.06 mm with CH, 0.77 ± 0.07 mm with CS, and 0.88 ± 0.05 mm in the control cells (**Fig. 8B**). This data suggests that the CH-CS PEC can support and stimulate the growth of the dermal fibroblasts and epidermal keratinocytes.

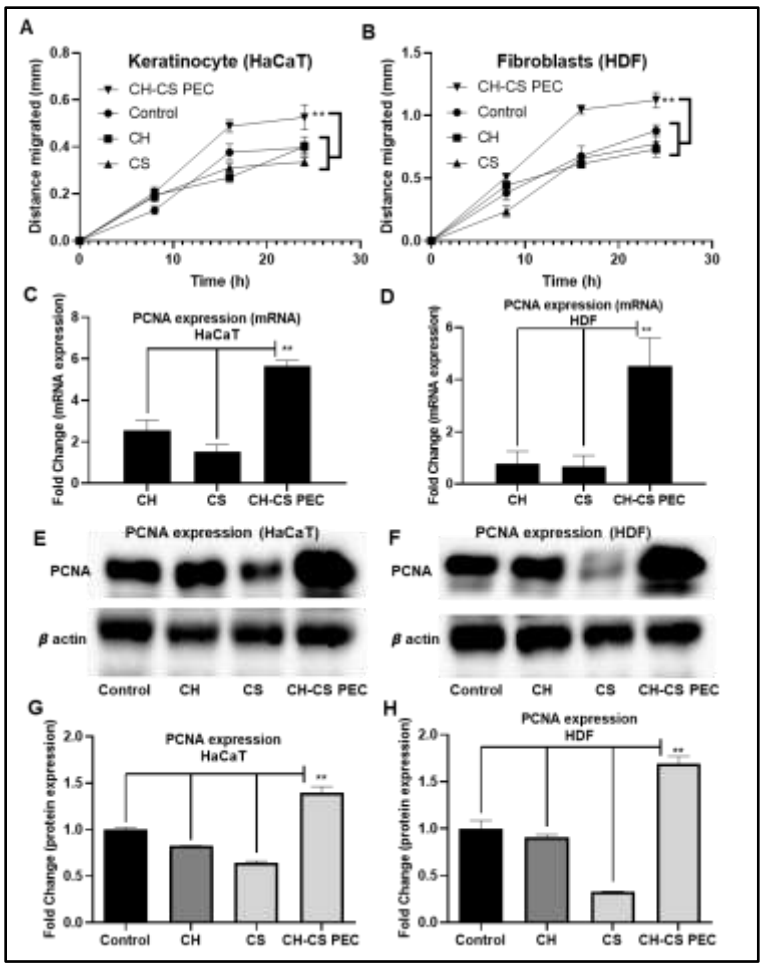

Fig. 8. Quantification of cell migration. **A** and **B**: Analysis of the distance migrated by both HaCaT and HDF cells grown on different polymeric scaffolds. Statistical analysis was done using 2-way ANOVA with Tukey multiple comparison test. ** denotes *p* value < 0.05. **C** and **D**: Evaluation of the expression of PCNA as a cell proliferation marker in the HaCaT and HDF cells qRT-PCR. **E** and **F**: Western blot analysis of PCNA expression in the HaCaT and HDF cells. **G** and **H**: Densitometric analysis of the PCNA western blot. Statistical analysis was done using 2-way ANOVA with Tukey multiple comparison test. ** denotes *p* value < 0.05.

2. Evaluation of the expression of proliferation markers by keratinocytes and fibroblasts

After observing enhanced cell migration with the CH-CS PEC, we evaluated the expression of proliferating cell nuclear antigen (PCNA) as a proliferation marker in both HaCaT and HDF cells by both real-time qPCR as well as western blot analysis. In the HaCaT cells, 5.6-fold increased expression of PCNA was observed in the CH-CS PEC group, compared to 2.5-fold in CH and 1.5-fold in CS (**Fig. 8C**). In the HDF cells, a 4.5-fold increase in PCNA expression was observed with the CH-CS PEC grown cells, compared to both CH (0.8-fold) and CS (0.7-fold) (**Fig. 8D**). The western blot of PCNA protein expression analysis also corroborates the qPCR data. A significantly increased PCNA expression was observed with both HaCaT and HDF cells grown on the CH-CS PEC compared to regular Petri plate, as well as with CH and CS treatment (**Fig. 8E-H**). PCNA expression was found to be increased by 1.4 and 1.7-fold in the HaCaT and HDF cells, respectively, when grown on the CH-CS PEC compared to the control. On the other hand, with the CH and CS treatment, PCNA expression was found to be slightly decreased compared to control [36], presence of a low viscoelastic polymer like CH or CS alone may adversely impact cell proliferation. The crosslinked CH-CS PEC, due to its higher viscoelasticity and porosity, could improve cell proliferation.

3. Evaluation of the expression of functional markers by keratinocytes and fibroblasts

Next, we studied the functional potential of these cells grown on the CH-CS PEC scaffold. Functionally active keratinocytes at the wound healing site get differentiated to express involucrin, a precursor of the epidermal cornified envelope [37]. In the current study, we observed only a basal level of involucrin expression with CH and CS treatment (less than 1-fold increase) at 48h. On the contrary, with CH-CS PEC, a 3.7-fold increase in involucrin expression was observed (**Fig. 9A**). Similar observations with CH film have been reported earlier as well [36]. Apart from involucrin, we have also analyzed the expression of HGF. HGF expression accelerates wound healing and reduces fibrosis [38], and promotes granulation tissue and angiogenesis [39]. With the CH-CS PEC treatment, a 6-fold increase in the expression of HGF was observed, compared to a 1.9-fold and 4.7-fold increase with CH and CS, respectively (**Fig. 9B**). These data indicated that the keratinocyte cells were functionally more active when grown on the CH-CS PEC.

We have also analyzed the scaffold seeded HaCaT cells' response treated with HDF conditioned media to evaluate the cellular crosstalk between keratinocytes and fibroblasts [40, 41]. It has been demonstrated that the expression of β1-integrin by the keratinocytes is augmented by factors secreted by the fibroblasts [42]. Cells grown on CH or CS expressed very low levels of β1-integrin (0.8 and 0.6-fold, respectively). In contrast, a 1.9-fold increase in the β1-integrin expression was observed with HaCaT cells grown on CH-CS PEC without conditioned media treatment, indicating that the interaction with the viscoelastic CH-CS PEC may enhance expression (**Fig. 9C**). Importantly, with HDF conditioned media treatment, HaCaT cells grown on CH-CS PEC exhibited a 3.5-fold increase in the expression of β1-integrin (**Fig. 9C**). In contrast, HaCaT cells grown in standard culture plate treated with HDF conditioned media showed only a basal level of β1-integrin expression (0.4-fold), suggesting the role of the CH-CS PEC scaffold for its expression, consistent with previous reports that a matrix structure is important for the expression of integrins [43, 44].

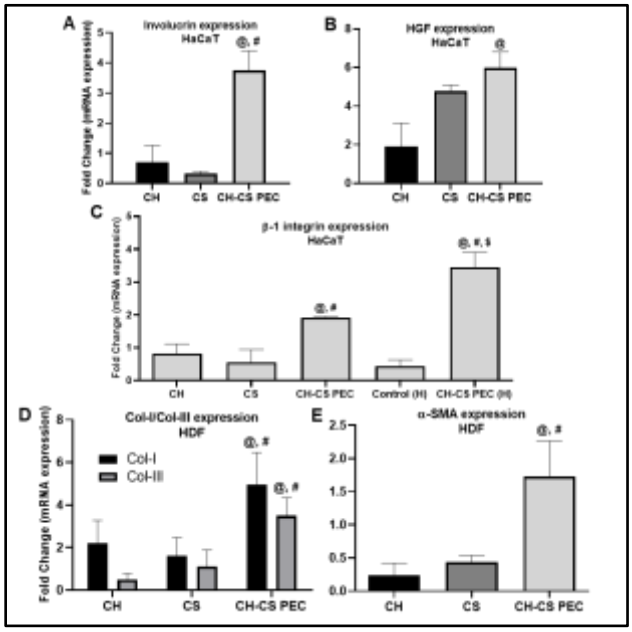

Fig. 9. qRT-PCR analysis of the expression of functional markers in the HaCaT and HDF cells treated with different polymeric scaffolds for 48h. In the HaCaT cells, the following markers were analyzed: **A:** involucrin, **B:** HGF, and **C:** β1-integrin. β1-integrin expression was compared with the CH-CS PEC grown cells treated with HDF conditioned media [CH-CS PEC(H)]. Control(H) denotes HaCaT cells grown on Petri plate treated with HDF conditioned media. In the HDF cells, the following markers were analyzed: **D**: Col-I and Col-III, and **E**: α-SMA. Statistical analysis was done using 1-way ANOVA with Tukey multiple comparison test. @ denotes p value < 0.05 compared to CH, # denotes p value < 0.05 compared to CS, $ denotes p value < 0.05 compared to CH-CS PEC.

Next, we studied the functional efficacy of another vital skin cell, fibroblasts, by analyzing the expression of collagen-I, collagen-III, and α-SMA as a functional marker. Fibroblasts are the principal skin cells responsible for generating the extracellular matrix (ECM) in the dermal tissue. There are various collagen typepresent in the skin, amongst the fibrillar collagens, type I (Col-I) and type III (Col-III) are the most predominant in the skin. Col-III helps in forming a provisional ECM structure at the early stage of wound healing [45]. Expression of Col-III also supports wound contraction [45]. Volk et al. have demonstrated increased scar tissue formation in Col-III deficient mice [46]. On the other hand, Col-I is mechanically stronger than Col-III and responsible for maintaining skin structure and tissue integrity [45]. Both the collagens play a vital role in the wound healing process. In our study, increased expression of both Col-I and Col-III was observed with the CH-CS PEC (Col-I: 3.8-fold, Col-III: 2.9-fold), compared to CH (Col-I: 0.4-fold, Col-III: 0.1-fold) and CS (Col-I: 1.8-fold, Col-III: 0.2-fold) (**Fig. 9D**). Interestingly, the Col-I to Col-III ratio was calculated to be 4:1 and 9:1 with CH and CS, respectively, while in the case of CH-CS PEC, it was 1.3:1. Though the mechanism is not clearly understood yet, the 1:1 ratio of Col-I to Col-III has been associated with scarless wound healing [45]. It has been shown that in the fetal skin, Col-I to Col-III ratio varies from 2.3:1 to 0.7:1, compared to 9:1 to 4:1 in the adult [47, 48]. The higher amount of Col-III expression by the wounded fetal skin may influence scarless wound healing seen in the fetus [48]. In the adult skin, scar tissue was found to have a Col-I to III ratio of 6:1 to 17:1 [49]. As with the CH-CS PEC treatment, the Col-I/III ratio was found to be almost 1:1, similar to that of the fetal skin, scarless wound healing could be possible with the CH-CS PEC.
Apart from Col-I and III, we have also analyzed the expression of α-SMA in fibroblasts. α-SMA expression is associated with the structural and mechanical properties of the matrix [50, 51] and is responsible for generating contractile force in the skin [52]. α-SMA is a marker of myofibroblasts, which are differentiated fibroblasts with smooth muscle-like features and play a significant role in the wound healing process [53]. We found a 1.7-fold increase in α-SMA expression with the CH-CS PEC treatment, whereas, with CH and CS it was 0.2 and 0.4-fold, respectively (**Fig. 9E**). These data suggest that the fibroblasts grown on the CH-CS PEC were functionally more active, which can benefit the wound healing process.

4. In-vitro macrophage infection model:

From our viscoelastic data we found the CH-CS PEC has good viscoelasticity and cells grown on the viscoelastic substrate has the tendency to show immunomodulatory effect. We found CH-CS PEC to have good antibacterial activity and now we wanted to check the effect change in macrophage response post infection with pseudomonas aeurignosa when these cells are treated with CH-CS PEC. For the initiation of the study we infected macrophages treated with CH, CS and CH-CS PEC with the bacteria with multiplicity index of 20. The results demonstrated decrease in the extracellular bacterial load CH-CS PEC treated macrophages **(Fig.10**) Next we checked the time dependent cytokine expression profile in uninfected, 3h post infection and 6h post infected cells. The results demonstrated time dependent change in the TNF-alpha and IL-10 expression in the macrophages. At 3h the macrophages are in pro- inflammatory state when treated with CHCS

PEC (IL10-2.27±1.25 and TNF-alpha-12.5±1.88). which is getting changed to anti-inflammatory state at 6h with increase expression of IL-10 and reduced expression of TNF-alpha(IL10-14.52±1.21 and TNF-alpha-0.91±1.25). Hence the results demonstrated the CH-CS PEC has both antibacterial and antinflammtory activity which could be beneficial in tissue repair process.(**Fig 10**)

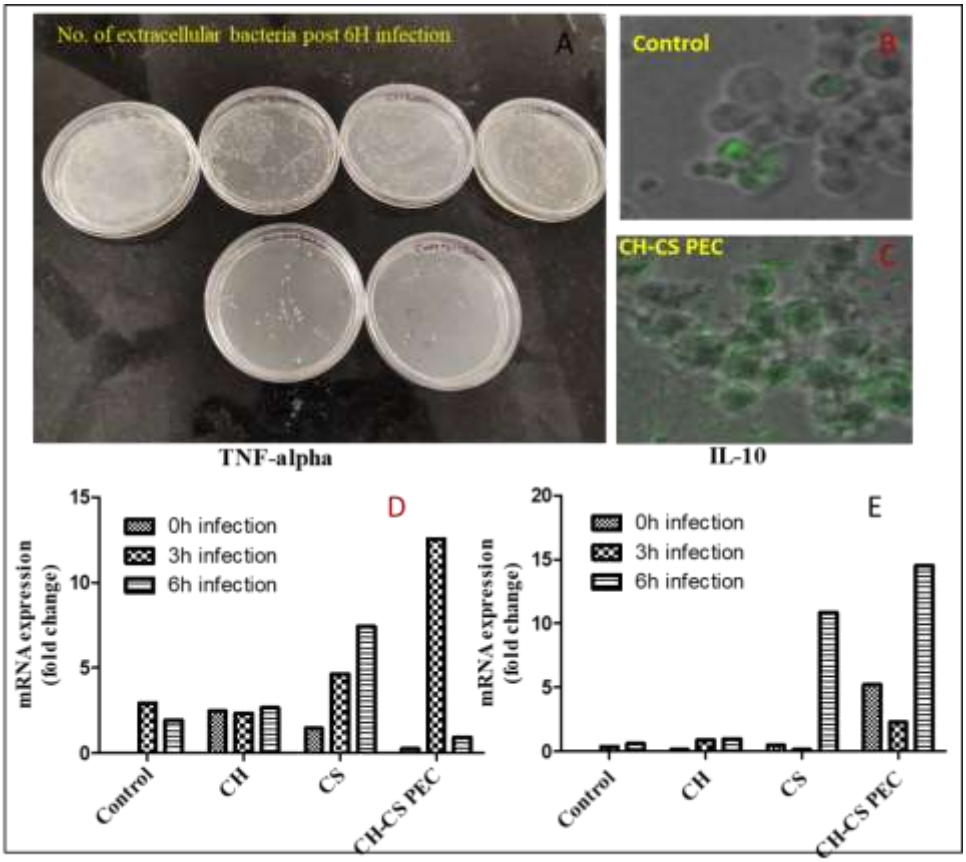

Fig.10. A) Extracellular bacterial growth post 6h infection**, B & C**)Internalization of GFP tagged bacteria to the macrophage post 6h infection and **D&E)** TNF-alpha and IL-10expression profile at 0h, 3h and 6h post infection

Objective 3: In-vivo wound healing study and determination of the molecular mechanism involved in the wound treated with simvastain loaded CH-CS PEC.

1. In-vivo wound healing efficacy:

After demonstrating enhanced cell proliferation and functional efficacy of keratinocytes, fibroblasts and macrophages treated with the CH-CS PEC, next we evaluated the *in-vivo* wound healing activity of the *in-situ* forming scaffold and compared it with the lyophilized CH-CS PEC, as well as a market available chitosan-based scaffold. The study was performed in the Wistar rats with a full-thickness excisional wound of 2×2 cm^2 area. The animals were divided into four groups,

untreated, lyophilized CH-CS PEC, *in-situ* CH-CS PEC, and a market available CH based preformed scaffold. *In-situ* CH-CS PEC treatment was given using a custom-made double-barreled syringe, with CH solution in one chamber and CS solution in the other chamber.For application, both the pistons of the double-barreled syringe were compressed simultaneously, leading to the ejection of both the solutions at the same rate. The wound healing was analyzed by taking the images of treated wounds every second day.

Compared to all others, significantly faster wound closure was observed with the *in-situ* CH-CS PEC group (**Fig. 11A** and **B**). At day 10, the mean % wound closer was calculated to be 89.5±0.26% with the *in-situ* CH-CS PEC, compared to 82.5±2.5%, 81.1±2.19%, and 74.2±1.98% with the lyophilized CH-CS PEC, marketed, and untreated control, respectively (**Fig. 11B**). Compared between the *in-situ* CH-CS PEC and the market available chitosan-based scaffold, the former exhibited significantly increased wound closure at the final time point, indicating the *in-situ* scaffold formation may improve the wound healing activity. The enhanced wound closure rate of *in-situ* CH-CS PEC could be due to CH and CS properties as well as because of the physicochemical properties of the CH-CS PEC *in-situ*, including enhanced support to the basement cells in the wound bed.

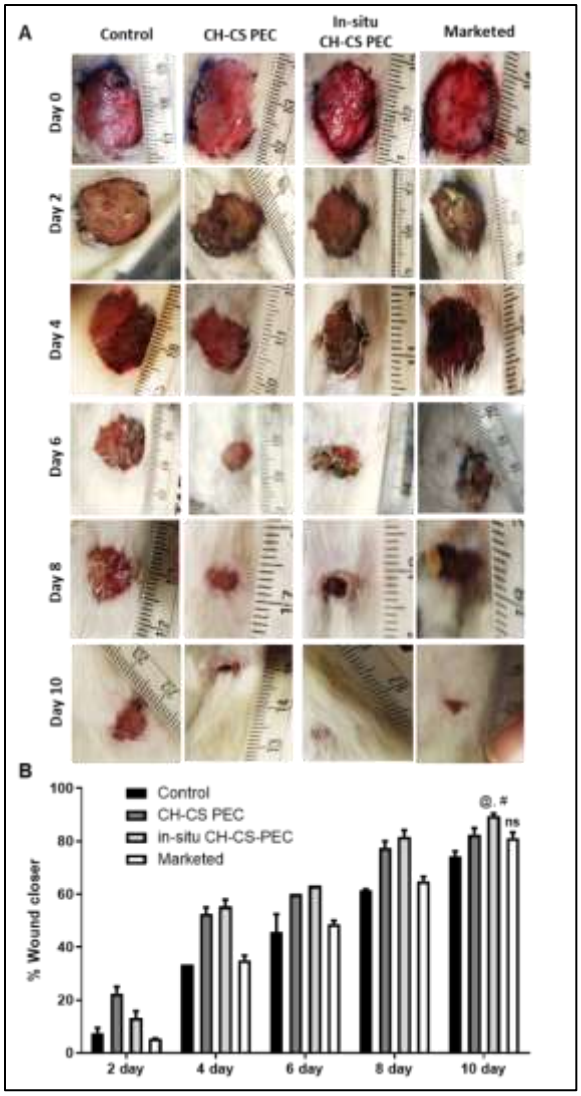

Fig. 11. **A**: In-vivo wound healing efficacy in rat excisional wound model. **B**: % Wound closer rate with different treatments. Statistical analysis was done using 2-way ANOVA with Tukey multiple comparison test. @ denotes *p* value < 0.05 compared to control, # denotes *p* value < 0.05 compared to marketed. ns: not significant compared to control.

2. Histology studies

After confirming efficient wound closure with the CH-CS PEC, histological evaluation of the wounds was performed 7-days and 14-days post-treatment in the four groups (**Fig. 12A**). On the 7^{th}-day post-treatment, a considerable amount of granulation tissue was observed in all the groups except the control, suggesting initiation of healing in the three groups. The control group exhibited the presence of granulation tissue as late as day 14, while the other three groups showed the presence of neo-epidermis formation and a healed dermal layer on the 14th day. Significantly improved re-epithelization was observed in the animals treated with the PEC scaffold and in-situ CH-CS PEC group compared to the market available chitosan-based scaffold treated group (broken epidermis marked with an arrow) (**Fig. 12A**). Dermal appendages were observed in all three treated groups, with most appendages seen in the in-situ CH-CS PEC group (marked with a star) (**Fig. 12A**). The amount of collagen deposited was performed by picrosirius staining of the skin section. **Fig. 12 B.**

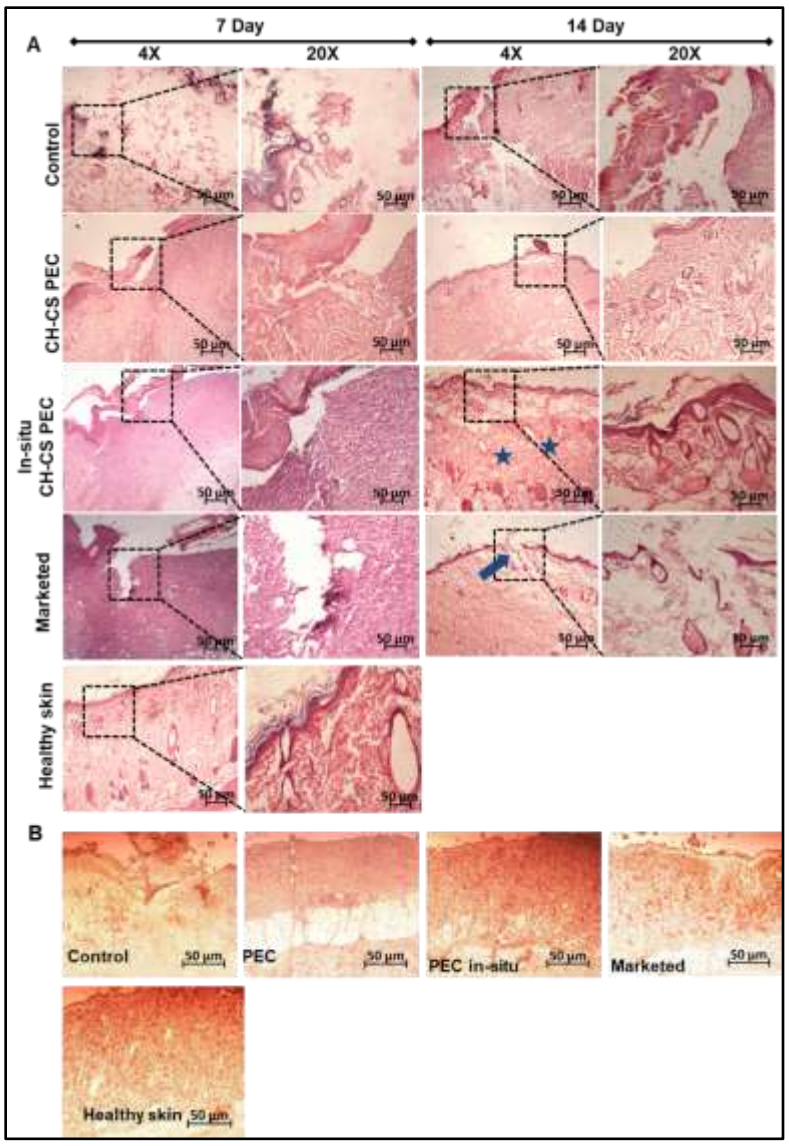

Fig. 12. **A**: Histopathological evaluation of the skin at 4X and 20X magnification, at 7th day and 14th day after the treatment. Scale bar 50 μm. **B**: Brightfield microscopic images of total collagen staining of the skin samples at 14th day post-treatment by picrosirius red staining. Scale bar 50 μm.

3. IHC analysis

After analyzing the efficient wound closure, and confirming the enhanced collagen content in the *in-situ* CH-CS PEC treated group, we wanted to analyze the molecular markers of wound healing in the treated animals. We evaluated the expression of α-smooth muscle actin (α-SMA) and β1-integrin in all the treated groups by immunohistochemical analysis. As depicted in **Fig. 13A**, the expression of α-SMA was minimal in the control group (32±2% of the healthy skin). No significant difference was found in the α-SMA level in the lyophilized CH-CS PEC (47±2%) as well as marketed product (42±4%) treatment groups compared to control (**Fig. 13A**). The level of α-SMA in the *in-situ* CH-CS PEC group was 75±9% of the healthy skin, significantly higher than the control (**Fig. 13A**). In the *in-vitro* study also, we have found enhanced expression of α-SMA by the CH-CS PEC seeded HDF cells (**Fig. 9E**). Expression of α-SMA indicates wound contraction

and faster granulation tissue formation, leading to faster cell proliferation and re-epithelialization [54].

We have also analyzed the expression of β1-integrin. As depicted in **Fig. 13B**, deficient expression was found in the control group (39±7% of the healthy skin). In the marketed CH scaffold treated group, only a moderate increase (statistically insignificant) in the β1-integrin expression was observed (55±3%). A significant increase was detected with the lyophilized CH-CS PEC treated group (67±7%) compared to the control; however, it was not significantly different from the marketed CH scaffold treated group. With the *in-situ* CH-CS PEC treatment, a significantly higher amount of β1-integrin was detected (78±3%) compared to the control and the marketed product. As observed in the *in-vitro* study also (**Fig. 9C**), the presence of a viscoelastic matrix-like structure can significantly improve the mechano-sensing by the cells, which can modulate the expression of β1-integrin [55, 56]. *In-situ* application of the CH-CS PEC directly at the wound bed can provide a viscoelastic scaffold for functional maturation of the wound bed cells, stimulating expression of markers like β1-integrin.

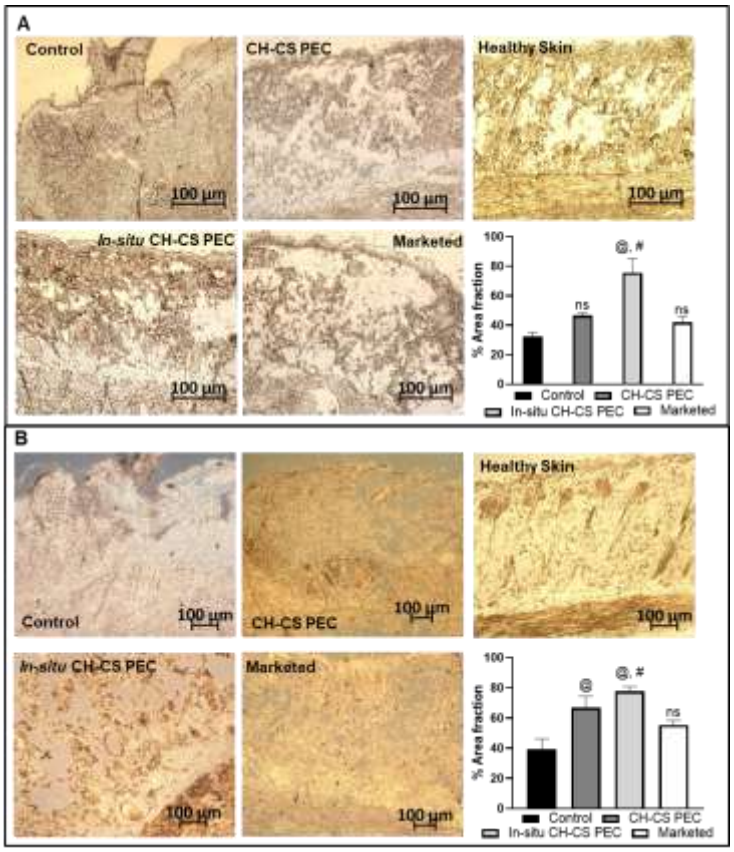

Fig. 11. Immunohistochemical staining of **A**: α-SMA and **B**: β1-integrin in the skin tissue sections collected 14th day post-treatment. The expression of the markers was compared with the skin section of the healthy skin. Scale bar 100 µm. Statistical analysis was done using 1-way ANOVA with Tukey multiple comparison test. @ denotes p value < 0.05 compared to control, # denotes p value < 0.05 compared to marketed. ns: not significant compared to control.

Discussion:

In-situ forming scaffolds could exhibit enhanced wound healing property due to their direct contact with the wound bed cells. Previous attempts for making *in-situ* wound healing scaffold involved chemical reactions, making them not suitable for clinical application. Also, complicated design makes their large-scale production very challenging [57-60]. In the present study, we have demonstrated that by electrostatic crosslinking, CH and CS solutions can form a crosslinked polymeric scaffold directly at the wound site, with no other chemicals or complicated modifications needed. This design simplicity is the most important feature of this scaffold. We have established a crosslinked scaffold formation by solid-state NMR, X-ray diffraction, and TGA analysis. The scaffold was found to have high viscoelastic property, with self-healing capability. It also significantly improved keratinocyte and fibroblast proliferation and function. In the rat skin-excisional wound model, treatment with the *in-situ* forming scaffold exhibited enhanced wound healing efficacy in terms of wound closure rate, collagen content, as well as α-SMA and β1-integrin expression.

Biocompatibility is a very important criteria for any wound healing scaffold. In our previous study, we have demonstrated the CH-CS PEC to be highly hemocompatibility [61]. As wound healing scaffolds directly come in contact with cells, one of the major toxicities is due to cell membrane destabilization. RBC has one of the weakest plasma membranes among all types of body cells. We have demonstrated that the CH-CS PEC does not cause hemolysis. In the current study, we have observed significantly increased proliferation and migration of both keratinocyte and fibroblast cells when grown on the CH-CS PEC, better than cells grown on Petri plates, indicating high compatibility of the scaffold to the skin cells. Furthermore, in the in-vivo study, the groups treated with CH-CS PEC (both lyophilized and in-situ forming) showed no redness or any other complications after treatment. Altogether, these data indicate high biocompatibility of the CH-CS PEC.

Altogether, this study demonstrated that mixing of CH and CS solution made a highly viscoelastic, porous scaffold, which can support epidermal and dermal cell proliferation and bio-function, with an enhanced *in-vivo* wound healing efficacy. The simplistic design strategy and easy preparation of this scaffold have substantial significance for possible clinical translation.

Impact of the research in the advancement of knowledge or benefit to mankind:

Many polymeric wound dressings are available, however all of them are prefabricated and henceforth limits their use as could not go deep into the crevices of the wound edge. These dressings effectively undergoes wound closure but limits the strength of the newly formed tissue and ends up in scar formation. Hence there is a need to make an effective formulation by which the benefits of these biopolymers could be utilized. In situ formation of the scaffold could maintain the moisture at the wound site which supports the healing process. We have developed an in-situ forming polysaccharide based bioscafold. The CH-CS PEC was prone to show good viscoelasticity which supported cellular growth functional efficacy of the dermal and epidermal cells. Alongwith this, we found this scaffold to have immunomodulatory activity towards macrophages. From our

Studies, we determined that the CH-CS PPEC has good wound healing efficacy on its own and is a good carrier for drug loading as well. Hence effective loading of an angiogenic molecule to the CH-CS PEC could lead to the dressing with overall wound healing efficiency with reduce scar formation.

References

1. Siddiqui, A.R. and J.M. Bernstein, *Chronic wound infection: facts and controversies.* Clin Dermatol, 2010. **28**(5): p. 519-26.
2. Dhivya, S., V.V. Padma, and E. Santhini, *Wound dressings - a review.* Biomedicine (Taipei), 2015. **5**(4): p. 22.
3. Agren, M.S. and M. Werthen, *The extracellular matrix in wound healing: a closer look at therapeutics for chronic wounds.* Int J Low Extrem Wounds, 2007. **6**(2): p. 82-97.
4. Kunkemoeller, B. and T.R. Kyriakides, *Redox Signaling in Diabetic Wound Healing Regulates Extracellular Matrix Deposition.* Antioxid Redox Signal, 2017. **27**(12): p. 823-838.
5. Eming, S.A., P. Martin, and M. Tomic-Canic, *Wound repair and regeneration: mechanisms, signaling, and translation.* Sci Transl Med, 2014. **6**(265): p. 265sr6.
6. Olczyk, P., L. Mencner, and K. Komosinska-Vassev, *The role of the extracellular matrix components in cutaneous wound healing.* Biomed Res Int, 2014. **2014**: p. 747584.
7. Schultz, G.S. and A. Wysocki, *Interactions between extracellular matrix and growth factors in wound healing.* Wound Repair Regen, 2009. **17**(2): p. 153-62.
8. Galkowska, H., W.L. Olszewski, and U. Wojewodzka, *Keratinocyte and dermal vascular endothelial cell capacities remain unimpaired in the margin of chronic venous ulcer.* Arch Dermatol Res, 2005. **296**(7): p. 286-95.
9. Tian, Y.W. and M.C. Stacey, *Cytokines and growth factors in keratinocytes and sweat glands in chronic venous leg ulcers. An immunohistochemical study.* Wound Repair Regen, 2003. **11**(5): p. 316-25.
10. Ahn, S., et al., *Soy Protein/Cellulose Nanofiber Scaffolds Mimicking Skin Extracellular Matrix for Enhanced Wound Healing.* Adv Healthc Mater, 2018. **7**(9): p. e1701175.
11. Dickinson, L.E. and S. Gerecht, *Engineered Biopolymeric Scaffolds for Chronic Wound Healing.* Front Physiol, 2016. **7**: p. 341.
12. Qin, X., et al., *An Extracellular Matrix-Mimicking Hydrogel for Full Thickness Wound Healing in Diabetic Mice.* Macromol Biosci, 2018. **18**(7): p. e1800047.

13. Zhu, C., et al., *Novel enzymatic crosslinked hydrogels that mimic extracellular matrix for skin wound healing.* Journal of Materials Science, 2018. **53**(8): p. 5909-5928.
14. Daristotle, J.L., et al., *Sprayable and biodegradable, intrinsically adhesive wound dressing with antimicrobial properties.* Bioeng Transl Med, 2020. **5**(1): p. e10149.
15. Hu, S., et al., *Preparation of composite hydroxybutyl chitosan sponge and its role in promoting wound healing.* Carbohydr Polym, 2018. **184**: p. 154-163.
16. Ong, S.Y., et al., *Development of a chitosan-based wound dressing with improved hemostatic and antimicrobial properties.* Biomaterials, 2008. **29**(32): p. 4323-32.
17. Golafshan, N., et al., *Nanohybrid hydrogels of laponite: PVA-Alginate as a potential wound healing material.* Carbohydr Polym, 2017. **176**: p. 392-401.
18. Sharma, S., et al., *Mechanically magnified chitosan-based hydrogel as tissue adhesive and antimicrobial candidate.* Int J Biol Macromol, 2019. **125**: p. 109-115.
19. Yasa, I., et al., *Assessment of antimicrobial activity of nanosized Ag doped TiO(2) colloids.* World J Microbiol Biotechnol, 2012. **28**(7): p. 2531-9.
20. Heux, L., et al., *Solid state NMR for determination of degree of acetylation of chitin and chitosan.* Biomacromolecules, 2000. **1**(4): p. 746-751.
21. Winter, W.T., et al., *Solid-state 13C NMR and X-ray diffraction of dermatan sulfate.* Biochem Biophys Res Commun, 1986. **137**(1): p. 87-93.
22. Eddya, M., B. Tbib, and K. El-Hami, *A comparison of chitosan properties after extraction from shrimp shells by diluted and concentrated acids.* Heliyon, 2020. **6**(2): p. e03486.
23. Ebube, N.K., W. Mark, and H. Hahm, *Preformulation studies and characterization of proposed chondroprotective agents: glucosamine HCl and chondroitin sulfate.* Pharm Dev Technol, 2002. **7**(4): p. 457-69.
24. Barroso, N., et al., *Self-healable hyaluronic acid/chitosan polyelectrolyte complex hydrogels and multilayers.* European Polymer Journal, 2019. **120**.
25. Smith, S.A., et al., *Dartintinnus alderae n. g., n. sp., a Brackish Water Tintinnid (Ciliophora, Spirotrichea) with Dual-ended Lorica Collapsibility.* J Eukaryot Microbiol, 2018. **65**(3): p. 400-411.
26. Hosseini, M.S. and A.A. Katbab, *Effects of surface viscoelasticity on cellular responses of endothelial cells.* Rep Biochem Mol Biol, 2014. **3**(1): p. 20-8.
27. Guimarães, C.F., et al., *The stiffness of living tissues and its implications for tissue engineering.* Nature Reviews Materials, 2020. **5**(5): p. 351-370.
28. Heidenreich, A.C., et al., *Collagen and chitosan blends for 3D bioprinting: A rheological and printability approach.* Polymer Testing, 2020. **82**: p. 106297.
29. Chan, B.P. and K.W. Leong, *Scaffolding in tissue engineering: general approaches and tissue-specific considerations.* Eur Spine J, 2008. **17 Suppl 4**: p. 467-79.
30. Zhang, A., et al., *Research status of self-healing hydrogel for wound management: A review.* Int J Biol Macromol, 2020. **164**: p. 2108-2123.
31. Yang, B., et al., *Injectable Adhesive Self-Healing Multicross-Linked Double-Network Hydrogel Facilitates Full-Thickness Skin Wound Healing.* ACS Appl Mater Interfaces, 2020. **12**(52): p. 57782-57797.
32. Panico, A., F. Paladini, and M. Pollini, *Development of regenerative and flexible fibroin-based wound dressings.* J Biomed Mater Res B Appl Biomater, 2019. **107**(1): p. 7-18.
33. Archana, D., et al., *Chitosan-PVP-nano silver oxide wound dressing: in vitro and in vivo evaluation.* Int J Biol Macromol, 2015. **73**: p. 49-57.
34. Lima, M.R., et al., *Evaluation of the interaction between polymyxin B and Pseudomonas aeruginosa biofilm and planktonic cells: reactive oxygen species induction and zeta potential.* BMC Microbiol, 2019. **19**(1): p. 115.
35. Roether, J., et al., *Microstructure, local viscoelasticity and cell culture suitability of 3D hybrid HA/collagen scaffolds.* PLoS One, 2018. **13**(12): p. e0207397.
36. Tchemtchoua, V.T., et al., *Development of a chitosan nanofibrillar scaffold for skin repair and regeneration.* Biomacromolecules, 2011. **12**(9): p. 3194-204.
37. Ghahary, A., et al., *Keratinocyte differentiation inversely regulates the expression of involucrin and transforming growth factor beta1.* J Cell Biochem, 2001. **83**(2): p. 239-48.
38. Dally, J., et al., *Hepatocyte Growth Factor Mediates Enhanced Wound Healing Responses and Resistance to Transforming Growth Factor-beta(1)-Driven Myofibroblast Differentiation in Oral Mucosal Fibroblasts.* Int J Mol Sci, 2017. **18**(9).

39. Chmielowiec, J., et al., *c-Met is essential for wound healing in the skin.* J Cell Biol, 2007. **177**(1): p. 151-62.
40. Wojtowicz, A.M., et al., *The importance of both fibroblasts and keratinocytes in a bilayered living cellular construct used in wound healing.* Wound Repair Regen, 2014. **22**(2): p. 246-55.
41. Werner, S., T. Krieg, and H. Smola, *Keratinocyte-fibroblast interactions in wound healing.* J Invest Dermatol, 2007. **127**(5): p. 998-1008.
42. Seeger, M.A. and A.S. Paller, *The Roles of Growth Factors in Keratinocyte Migration.* Adv Wound Care (New Rochelle), 2015. **4**(4): p. 213-224.
43. Vecino, E., et al., *Influence of extracellular matrix components on the expression of integrins and regeneration of adult retinal ganglion cells.* PLoS One, 2015. **10**(5): p. e0125250.
44. Delcommenne, M. and C.H. Streuli, *Control of integrin expression by extracellular matrix.* J Biol Chem, 1995. **270**(45): p. 26794-801.
45. Xue, M. and C.J. Jackson, *Extracellular Matrix Reorganization During Wound Healing and Its Impact on Abnormal Scarring.* Adv Wound Care (New Rochelle), 2015. **4**(3): p. 119-136.
46. Volk, S.W., et al., *Diminished type III collagen promotes myofibroblast differentiation and increases scar deposition in cutaneous wound healing.* Cells Tissues Organs, 2011. **194**(1): p. 25-37.
47. Lovvorn, H.N., 3rd, et al., *Relative distribution and crosslinking of collagen distinguish fetal from adult sheep wound repair.* J Pediatr Surg, 1999. **34**(1): p. 218-23.
48. Hallock, G.G., et al., *Analysis of collagen content in the fetal wound.* Ann Plast Surg, 1988. **21**(4): p. 310-5.
49. Verhaegen, P.D., et al., *Differences in collagen architecture between keloid, hypertrophic scar, normotrophic scar, and normal skin: An objective histopathological analysis.* Wound Repair Regen, 2009. **17**(5): p. 649-56.
50. Jester, J.V., et al., *TGFbeta induced myofibroblast differentiation of rabbit keratocytes requires synergistic TGFbeta, PDGF and integrin signaling.* Exp Eye Res, 2002. **75**(6): p. 645-57.
51. Serini, G., et al., *The fibronectin domain ED-A is crucial for myofibroblastic phenotype induction by transforming growth factor-beta1.* J Cell Biol, 1998. **142**(3): p. 873-81.
52. Hinz, B., et al., *Alpha-smooth muscle actin expression upregulates fibroblast contractile activity.* Mol Biol Cell, 2001. **12**(9): p. 2730-41.
53. Chitturi, R.T., et al., *The role of myofibroblasts in wound healing, contraction and its clinical implications in cleft palate repair.* J Int Oral Health, 2015. **7**(3): p. 75-80.
54. Martinelli-Klay, C.P., et al., *Modulation of MCP-1, TGF-beta1, and alpha-SMA Expressions in Granulation Tissue of Cutaneous Wounds Treated with Local Vitamin B Complex: An Experimental Study.* Dermatopathology (Basel), 2014. **1**(2): p. 98-107.
55. Yeh, Y.C., et al., *Mechanotransduction of matrix stiffness in regulation of focal adhesion size and number: reciprocal regulation of caveolin-1 and beta1 integrin.* Sci Rep, 2017. **7**(1): p. 15008.
56. Sun, Z., S.S. Guo, and R. Fassler, *Integrin-mediated mechanotransduction.* J Cell Biol, 2016. **215**(4): p. 445-456.
57. Tsang, V.L. and S.N. Bhatia, *Three-dimensional tissue fabrication.* Adv Drug Deliv Rev, 2004. **56**(11): p. 1635-47.
58. Wang, P., et al., *In situ formed anti-inflammatory hydrogel loading plasmid DNA encoding VEGF for burn wound healing.* Acta Biomater, 2019. **100**: p. 191-201.
59. Griffin, D.R., et al., *Accelerated wound healing by injectable microporous gel scaffolds assembled from annealed building blocks.* Nat Mater, 2015. **14**(7): p. 737-44.
60. Ryan, C.N.M., M.N. Doulgkeroglou, and D.I. Zeugolis, *Electric field stimulation for tissue engineering applications.* BMC Biomed Eng, 2021. **3**(1): p. 1.
61. Sharma, S., K.L. Swetha, and A. Roy, *Chitosan-Chondroitin sulfate based polyelectrolyte complex for effective management of chronic wounds.* Int J Biol Macromol, 2019. **132**: p. 97-108.